Applied Physics Letters

Temperature and angle dependent magnetic imaging of biological iron nanoparticles using quantum diamond microscopy

Cite as: Appl. Phys. Lett. **122**, 032404 (2023); https://doi.org/10.1063/5.0114998
Submitted: 26 July 2022 • Accepted: 29 December 2022 • Published Online: 18 January 2023

R. W. de Gille, A. J. Healey, I. O. Robertson, et al.

AIP Publishing

Applied Physics Letters ARTICLE scitation.org/journal/apl

Temperature and angle dependent magnetic imaging of biological iron nanoparticles using quantum diamond microscopy

Cite as: Appl. Phys. Lett. **122**, 032404 (2023); doi: 10.1063/5.0114998
Submitted: 26 July 2022 · Accepted: 29 December 2022 ·
Published Online: 18 January 2023

R. W. de Gille,[1] A. J. Healey,[1] I. O. Robertson,[2] L. T. Hall,[3] J.-P. Tetienne,[2] E. P. Malkemper,[4] D. A. Keays,[5,6,7] L. C. L. Hollenberg,[1,8] and D. A. Simpson[1,a)]

AFFILIATIONS

[1]Department of Physics, University of Melbourne, Parkville, Victoria 3010, Australia
[2]School of Science, RMIT University, Melbourne, Victoria 3001, Australia
[3]Department of Chemistry, University of Melbourne, Parkville, Victoria 3010, Australia
[4]Max Planck Research Group Neurobiology of Magnetoreception, Max Planck Institute for Neurobiology of Behavior–caesar, Ludwig-Erhard-Allee 2, 53175 Bonn, Germany
[5]Institute for Molecular Pathology, Campus Vienna Biocenter 1, Vienna 1030, Austria
[6]Department of Anatomy and Neuroscience, University of Melbourne, Parkville, Victoria 3010, Australia
[7]Division of Neurobiology, Department Biology II, Ludwig-Maximilians-University Munich, Planegg-Martinsried, Munich 82152, Germany
[8]Centre for Quantum Computation and Communication Technology, University of Melbourne, Parkville, Victoria 3010, Australia

[a)]**Author to whom correspondence should be addressed:** simd@unimelb.edu.au

ABSTRACT

Quantum diamond microscopy is an emerging versatile technique for studying the magnetic properties of materials. It has been applied extensively in condensed matter physics and materials science and has blossomed into a unique platform for the magnetic study of biological systems. To date, biological demonstrations of quantum diamond microscopy have been performed under ambient conditions. Here, we extend this magnetic microscopy platform to cryogenic temperatures to study magnetic anisotropy and the blocking temperature from an individual iron organelle found within the inner ear of pigeons. Our work confirms that the interface between thin histological tissue sections and diamond can be maintained under cryogenic temperatures. Our magnetic images provide evidence of magnetic anisotropy from a single iron organelle with sub-cellular resolution using this correlative optical imaging method. This approach may be extended to a broad range of systems where magnetic materials play structural and functional roles in biological systems.

Iron is a crucial element for the structure and function of living systems. Our current understanding of bio-engineered iron materials has been shaped by techniques that allow us to probe the elemental structure and magnetic properties of these materials. The majority of magnetic studies into bio-engineered iron minerals have been undertaken using vibrating sample magnetometry and Mössbauer spectroscopy.[1,2] These studies typically require the magnetic material to be excised from the biological sample with large numbers of particles required to achieve sufficient magnetic sensitivity. This has two main limitations in the study of biological systems. Excising the magnetic material from the biological tissue is prone to sample contamination, and moving the magnetic material removes the possibility of correlating the magnetic properties back to a precise anatomical location within the tissue sample.[3] Alternate high resolution magnetic imaging platforms, such as nanoSQUIDs and magnetic force microscopy, have been developed and applied to study the magnetic properties of 2D and 3D materials.[4] Application of these magnetic imaging platforms to biological systems suffers several limitations. For example, magnetic force microscopy is a scanning technique, resulting in large measurement times in cases where biomagnetic particles are sparsely populated,[5] while using an array of SQUIDs instead of a scanning SQUID reduces the spatial resolution achievable with the technique.[6]

The negatively charged nitrogen-vacancy (NV) center in diamond is an optical color center, which is used as a sensitive and

versatile magnetic field sensor and has found numerous applications in biology.[7–10] Single NV centers in diamond have been used to probe the temperature dependent magnetic properties of single iron containing proteins such as ferritin.[11] The efficacy of the single NV approach depends on there being a sufficient density of proteins on the diamond surface to ensure an adequate magnetic interaction between the single NV center and the target molecule or complex. For biological tissue samples, where iron biominerals are sparsely distributed, an alternate approach is required. To complement these technologies, we adapt quantum diamond microscopy methods[12–16] to demonstrate that this platform is suitable to characterize thin histological samples of biological tissue at cryogenic temperatures with controlled background magnetic fields. The acquisition of high resolution magnetic images across the entire sample surface mitigates problems arising from limited magnetic interaction between an individual NV and a magnetic sample of interest. Furthermore, the transparency of diamond allows brightfield images of the biological tissue to be performed, which enables particular regions of interest to be identified. The optical nature of the imaging method conveniently allows the magnetic signals identified in a biological sample to be correlated to the anatomical location, thereby reducing the likelihood of false positives. The diffraction limited spatial resolution and parallel imaging also allow for wide fields of view to be explored over relatively short times compared to the aforementioned scanning techniques.

In this work, we prepare thin histological sections of the pigeon inner ear. These sections are known to contain small numbers of subcellular iron-based organelles referred to as cuticulosomes. We apply quantum diamond microscopy to study the magnetic properties of these materials from ambient to cryogenic temperatures to explore the blocking temperature and magnetic anisotropy of these organelles. Magnetic microscopy is performed down to 15 K which covers the estimated blocking temperature for iron biominerals, such as ferrihydrite. The thin histological sections of the inner ear are transferred onto a 100 μm thick diamond sensing chip, which contains a 2D layer of negatively charged nitrogen-vacancy (NV) centers at a depth of 10 nm and with an areal density of 10^{11} cm^{-2}.[17,18] The NV layer was engineered by implanting nitrogen ions into an electronic grade diamond with an energy of 4 keV and a dose of 10^{13} cm^{-2}. The diamond was subsequently annealed at 1000 °C in vacuum for a duration of 4 h to maximize NV center generation. The array of NV centers is used to produce 2D stray magnetic field images of the biological tissue sample. The magnetic images can be recorded from room temperature down to 15 K using our custom widefield quantum diamond microscope. The cryogenic system is equipped with a vector magnet that can apply an oriented background magnetic field up to 2500 G, along any of the four NV ⟨111⟩ crystallographic axis. By varying the temperature and applied background magnetic field, we can probe the magnetic anisotropy and blocking temperature of individual iron cuticulosomes located within the inner ear of a pigeon.

To perform magnetic microscopy, we start by preparing 500 nm thick histological samples taken from the lagena of adult pigeons as described in the Experimental Details section of the supplementary material. Tissue sections were transferred individually onto the diamond imaging chips via a drop of bi-distilled water using a small wire loop to hold the tissue sample. Sections were air-dried under a stereomicroscope to ensure flat mounting, with the flatness of the sample mount being checked following cooling and reheating. The diamond imaging chip contains a layer of NV centers located approximately 10 nm below the surface as shown in the inset of Fig. 1(a). Figure 1(b) shows a schematic diagram of the NV center in diamond and its

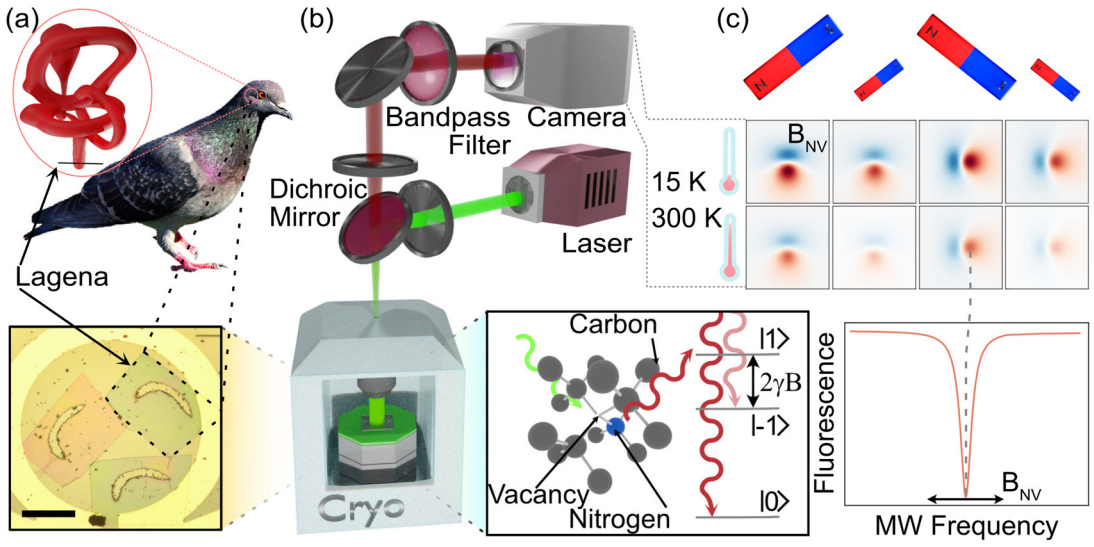

FIG. 1. Experimental design. (a) Thin sections were taken from the lagena of a pigeon and transferred to diamond imaging chips. The scale bar represents 0.5 mm. (b) The diamond and sample is placed in a cryogenic fridge. A 532 nm excitation laser is used to initialize and read the spin state of the NV centers. The diamond imaging chip sits atop a glass coverslip onto which a gold microwave resonator is printed to provide spin state control. A dichroic mirror is used to separate the NV fluorescence from the excitation. The NV fluorescence is imaged on an sCMOS camera. Fluorescence maps imaged under carefully designed NV spin state control schemes allow for maps of the magnetic field at the NV layer to be produced. The inset presents a schematic of an NV center in diamond. (c) Optically Detected Magnetic Resonance (ODMR) is performed over temperatures ranging from room temperature to 15 K and over a range of applied magnetic fields. Fluorescence drops occur where the microwave frequency relates to a transition between the $|0\rangle$ and $|\pm1\rangle$ spin sub-levels and magnetic field maps are calculated from resonant frequency maps.

associated ground state spin levels. The NV center is typically excited off resonantly using 532 nm excitation. The resulting fluorescence has a zero-phonon line at 637 nm and a broad phonon assisted sideband extending out to 800 nm. Optical spin state initialization and readout is enabled by a non-fluorescent decay route which is coupled to the $|\pm1\rangle$ spin states of the excited state manifold and the $|0\rangle$ spin state of the ground state manifold. This combination of properties is leveraged to precisely determine the position of the ground state $|\pm1\rangle$ levels using a protocol known as optically detected magnetic resonance (ODMR).[19] The $|\pm1\rangle$ spin states of the NV center Zeeman split in the presence of a magnetic field with a gyromagnetic ratio of $\gamma_{NV} = 2.8033$ MHz G^{-1}.[20] We take advantage of this property to report local magnetic fields experienced by ensembles of NV centers within the sensing layer. Stray magnetic field images are obtained by measuring the ODMR spectra at each imaging pixel using a custom widefield microscope. The widefield microscope separates the NV fluorescence from the excitation light via a dichroic mirror and a 650–750 nm bandpass filter. The resulting NV fluorescence image is captured using an sCMOS camera, as shown in Fig. 1(b). The ODMR spectrum is obtained by taking a series of NV fluorescence images while stepping through a range of microwave frequencies as described in de Gille *et al.*[16]

We start by obtaining stray magnetic field images of the thin histological sections at room temperature before transferring the sample to our cryogenic widefield microscope where the same series of experiments are repeated at temperatures down to 15 K. Brightfield images were taken before and after the measurements and no evidence of delamination or other temperature induced sample deterioration was observed. Furthermore, the sensitivity and resolution of the magnetic microscope was maintained at cryogenic temperatures, confirming the integrity of the interface between the histological section and the diamond surface. The stray magnetic field maps were obtained over a range of applied magnetic field strengths (30–2500 G), directions (the four $\langle 111\rangle$ crystallographic orientations of diamond), and temperatures (15–330 K) as indicated in the schematic shown in Fig. 1(c).

Cuticulosomes are quasi-spherical iron-rich structures located within the sensory hair cells in the inner ear of a range of avian species and were reported subsequent to the inner ear being implicated in pigeon magnetoreception.[1,16,21] Our previous work, conducted at ambient temperatures and with a fixed magnetic field alignment, measured the magnetic susceptibility of individual cuticulosomes.[16] Here, we explore the magnetic properties under various applied background field strengths and orientations at cryogenic temperatures to probe the level of magnetic anisotropy from an individual sub-micron magnetic particle.

We begin the magnetic characterization by obtaining a series of stray magnetic fields maps from an individual cuticulosome with a background field ($B_0 = 2500$ G) aligned along each of the four NV crystallographic axes at 15 K. The low temperatures at which the measurement was undertaken enabled the use of a superconducting vector magnet, allowing for precise magnetic field alignment to be achieved within minutes. The resulting magnetic images are shown in Fig. 2(a). Figure 2(b) presents linecuts taken through the corresponding stray magnetic field images. The double Gaussian fits provide a metric to quantify the strength of the stray magnetic field. The spatial profile and stray magnetic field strength is found to be dependent on the angle of the applied B_0, indicating that magnetic anisotropy is present in an individual cuticulosome. The magnetic anisotropy can originate from one or a combination of magnetocrystalline effects, shape anisotropy, and surface effects. To understand the observed magnetic anisotropy, we adapt the theoretical model that we developed in our previous work,[16] which describes the magnetic interaction between an iron cuticulosome and the NV sensing layer. We begin with a simulation of a single cuticulosome with no magnetic anisotropy. The simulation parameters are as follows: cuticulosome diameter d = 365 nm,[21] distance above the above the diamond NV sensing layer h = 215.5 nm, an applied $B_0 = 2500$ G, and a volume susceptibility, $\chi_v = 0.095$. The magnetic field at the NV layer due to a cuticulosome was then calculated as a dipole field,

$$\mathbf{B}_c(\mathbf{r}) = \frac{\chi_v V B_0}{4\pi}\left(\frac{3\mathbf{r}(\hat{\mathbf{m}}\cdot\mathbf{r})}{r^5} - \frac{\hat{\mathbf{m}}}{r^3}\right), \tag{1}$$

where $\hat{\mathbf{m}}$ is the magnetization direction of the cuticulosome, and V is the volume of the cuticulosome.

The model was then extended to include magnetic anisotropy by separating the magnetic susceptibility of individual iron complexes, which comprise a single cuticulosome into components aligned parallel and perpendicular to the easy axis of the particle. Simulations were performed by varying the easy axis and degree of magnetic anisoptropy to obtain qualitative agreement between the simulated outputs and the measured magnetic field images [see Figs. 2(c) and 2(d)]. In this implementation, the uncertainty in the height of the cuticulosomes above the NV layer and the radius of the particle inhibits the determination of a unique parameter set which best matches the experimental data; however, the model supports the qualitative finding of magnetic anisotropy within the magnetic material and sets a lower bound of the magnetic anisotropy of the cuticulosome of $\frac{\chi_a}{\chi_b} > 2$, where χ_a and χ_b are the magnetic susceptibilities along the easy and hard axes, respectively.

The temperature dependence of the magnetic properties of an individual cuticulosome can provide additional insight into its composition. In particular, the blocking temperature of a material details the temperature at which the magnetization becomes fixed and can be interpreted using Néel relaxation theory. The relaxation time of the magnetic moment of a uniaxial magnetic particle is given by

$$\tau = \tau_0 \exp\left(\frac{KV}{k_B T}\right), \tag{2}$$

where τ_0 is the pre-exponential factor, K is the constant of anisotropy, V is volume, k_B is Boltzmann's constant, and T is temperature.[22]

The temperature and volume of a magnetic particle impact the rate at which its magnetization flips. The specific combination of these two parameters that prevent magnetization flipping over a given time frame are known as the blocking temperature and volume, respectively (see the supplementary material for magnetic fluctuation spectra of iron oxide minerals). In terms of biogenic iron complexes, ferrihydrite is known to exist with granule sizes in a range between 1.5 and 10 nm resulting in blocking temperatures of 25 K.[23,24] Dynamic light scattering experiments performed on biogenic magnetite crystals have revealed size distributions ranging from 5 to 18 nm,[25] corresponding to a blocking temperature range of 12–85 K. Our previous work indicates that the magnetic susceptibility of cuticulosomes is greater than would be achieved from a solid sphere packed with ferrihydrite and

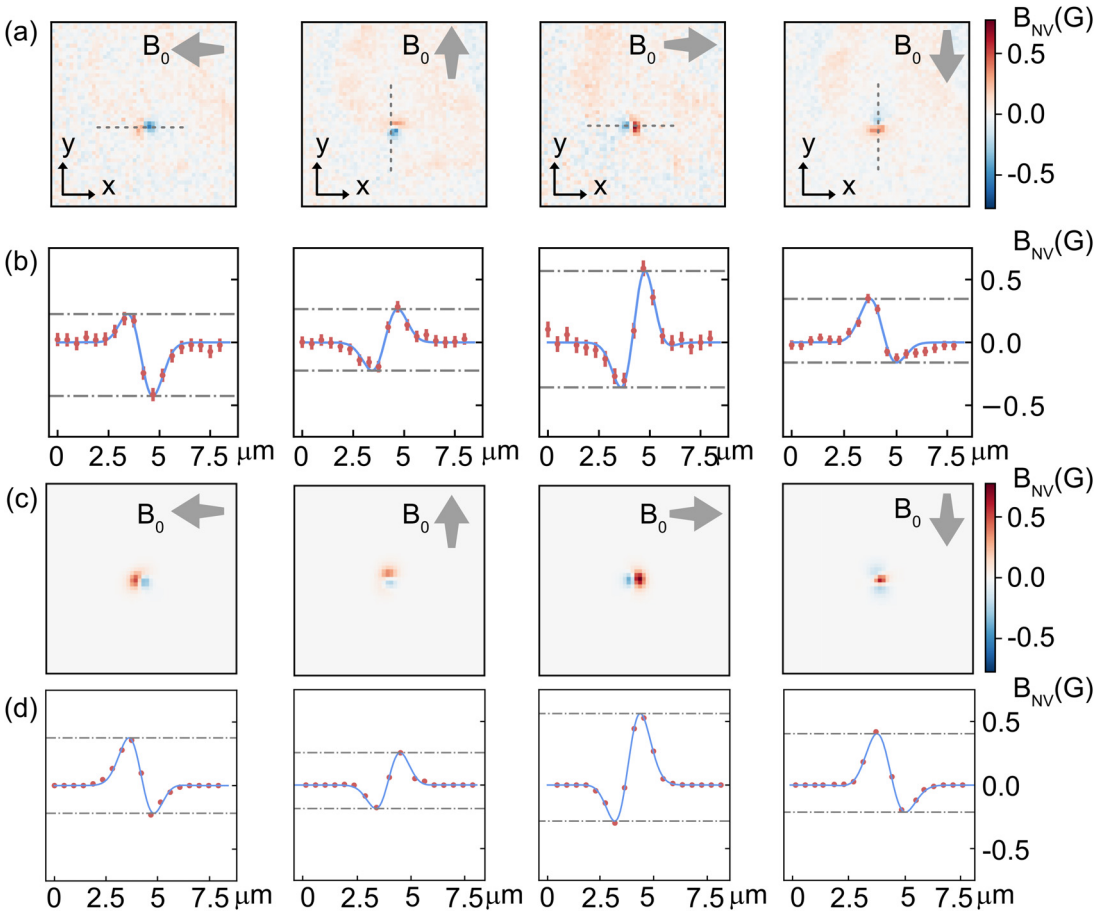

FIG. 2. Magnetic anisotropy is investigated by implementing ODMR with four distinct applied field directions at 15 K. (a) Each of the four frames corresponds to the applied magnetic field $B_0 = 2500$ G being aligned with one of the four diamond crystallographic axes. The gray arrows represent the projection of the applied magnetic field on the x–y plane. (b) Linecuts taken through the center of magnetic features with a double Gaussian fit. (c) Simulated stray magnetic field image of an anisotropic magnetic particle with an applied magnetic field aligned along each of the four crystallographic axes. (d) Linecuts taken through the simulated magnetic features. The side length of all images is 13 μm.

less than a solid sphere of magnetite.[16] The susceptibility measurements corroborated studies conducted by Nimpf *et al.* which found that cuticulosomes are likely to contain multiple iron oxide species.[26] To investigate the blocking temperature of an individual cuticulosome we applied a background magnetic field, $B_0 = 2500$ G, along a single NV axes at 15 K and measured the resulting stray magnetic field as shown in Fig. 3(a). The strength of the applied magnetic field was then reduced to 35 G, and the stray magnetic field from the particle re-measured [see Fig. 3(b)]. The linecuts taken through the particle are shown in Fig. 3(c) and reveal no remnant stray magnetic field at 15 K with an applied field of $B_0 = 35$ G. This indicates that the magnetization is relaxing on a timescale much faster than the acquisition time of the measurement, in this case, 120 min or 10^{-4} Hz. This result indicates a maximum possible magnetite crystal size of 9.4 nm and is consistent with the mounting evidence that these particles contain multiple iron oxide phases.

Finally, the stray magnetic field amplitudes as a function of applied field were measured at 15 and 300 K and are shown in Fig. 3(d). The magnetic response from the cuticulosome at both temperature indicates that T_B is below the temperatures reached. However, we note that the temperature within the tissue sample is a best estimate based on previous measurements using the same temperature sensor configuration and may differ slightly (<10 K) from the true temperature.[27]

In this work, we demonstrate how quantum diamond microscopy can be applied to image and characterize magnetic material found within thin biological tissue samples across a wide temperature range. In particular, we show how this imaging method can be applied to study the magnetic anisotropy and magnetic relaxation of subcellular magnetic particles found within the inner ear of pigeons. The observed anisotropy in these materials may arise from the presence of a shape anisotropy, magnetocrystalline effects, surface effects, or a combination thereof. We develop a semi-analytic model to predict the level of magnetic anisotropy based on varying magnetic contributions from elements aligned parallel and perpendicular to the easy axis of a single iron cuticulosome. The model provides qualitative agreement

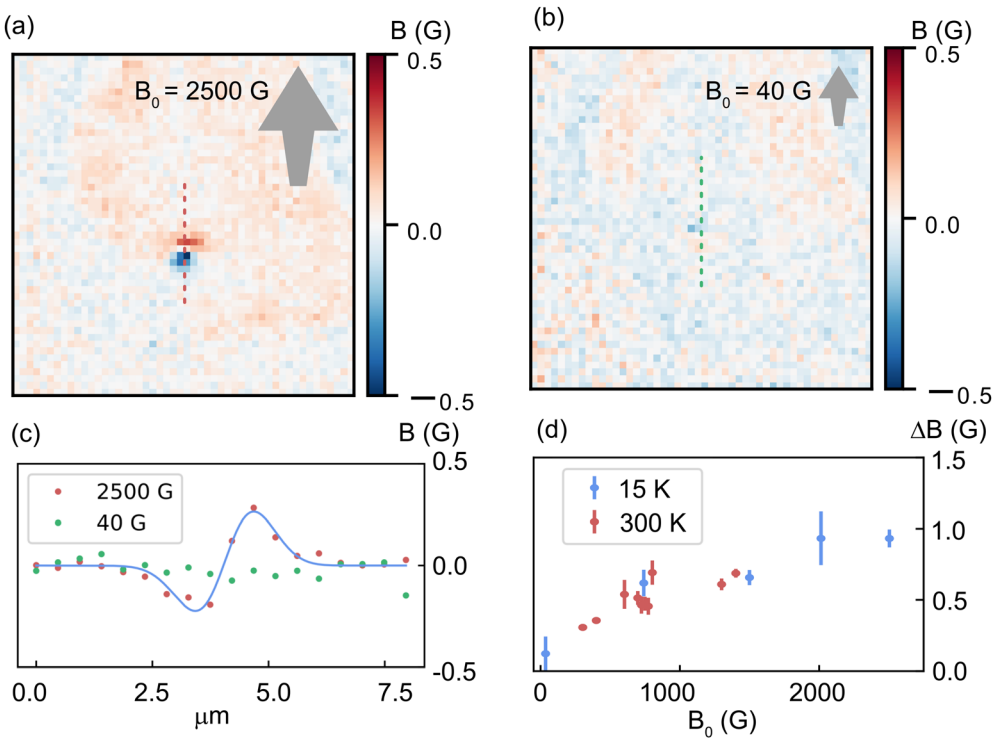

FIG. 3. Temperature dependent magnetic properties of cuticulosomes. (a) Stray magnetic field produced by a cuticulosome at 15 K with an applied magnetic field of 2500 G. (b) Stray magnetic field produced by a cuticulosome at 15 K with an applied magnetic field of 40 G. (c) Linecut through the magnetic feature. A double Gaussian function is fit to the data to extract a measure of the strength of the stray magnetic field. (d) Stray magnetic field strength vs applied magnetic field taken from the same cuticulosome at room temperature and at 15 K. Images are 13 × 13 μm^2 in size.

with the measured stray magnetic fields from the cuticulosomes. Further investigation into the magnetic susceptibility of these particles showed no discernible difference in the susceptibility measured at 15 K vs room temperature, suggesting that the blocking temperature of these materials is lower than that achieved in this work. The methodology employed here can be replicated to analyze other sub-micron magnetic structures where the anisotropy barrier and magnetic anisotropy are unknown. Cuticulosomes gained initial research interest as a potential site of magnetic particle mediated magnetoreception.[21] Although cuticulosomes do not appear to have a sufficiently large magnetic susceptibility to mediate a magnetoreceptive response, measurement of both magnetic susceptibilities and magnetic anisotropies is important for the analysis of other putative particle based magnetoreceptors.[3] There is scope for the technique developed here to be used in concert with techniques used to analyze particle size and shape, as magnetic anisotropy, magnetic relaxation, and particle geometry are interrelated properties. Examples of which include the study of thin films,[28] magnetic geological samples,[29] and the study of single superparamagnetic nanoparticles.[30] Future advancements of the method introduced here include increasing the brightness of the quasi 2D NV layer by increasing the thickness and density through multiple ion implantation runs or via controlled CVD growth and subsequently electron irradiation. The application of alternate optical and microwave pulse sequences may also be applied to reduce the measured ODMR linewidths allowing greater magnetic sensitivity. Methods to determine the distance between the sensing layer and magnetic particles would allow more precise determination of the magnetic properties of the particle and will be explored in future work. The successful interfacing of biological tissue samples with the diamond imaging chip at cryogenic temperatures does, however, show that quantum diamond microscopy has an important role to play in the characterization of a host of bio-magnetic materials.

See the supplementary material for further description of experimental details and the theoretical modeling.

The authors acknowledge support from the Australian Research Council (ARC) through various fellowships: L.T.H. (DE200101785) and J.-P.T. (FT200100073). L.C.L.H. is supported by CE170100012. R.W.d.G., I. O. R. and A.J.H. are supported by an Australian Government Research Training Program Scholarship. D.A.K. is supported by the European Research Council (ERC; Nos. 336725 and 819336) and the FWF (Y726). E.P.M. is supported by the Max Planck Society and the European Research Council (ERC; No. 948728).

AUTHOR DECLARATIONS

Conflict of Interest

The authors have no conflicts to disclose.

Ethics Approval

Ethics approval for experiments reported in the submitted manuscript on animal subjects was granted. All experiments were performed in accordance with an existing ethical framework (GZ:214635/2015/20) granted by the City of Vienna (Magistratsabteilung 58).

Author Contributions

Robert W. de Gille: Conceptualization (equal); Data curation (lead); Formal analysis (lead); Investigation (lead); Methodology (equal); Software (lead); Writing – original draft (equal); Writing – review & editing (equal). **A. J. Healey:** Data curation (supporting); Investigation (supporting); Methodology (supporting); Writing – review & editing (supporting). **I. O. Robertson:** Data curation (supporting); Investigation (supporting); Methodology (supporting); Writing – review & editing (supporting). **L. T. Hall:** Conceptualization (supporting); Data curation (supporting); Formal analysis (supporting); Funding acquisition (supporting); Investigation (supporting); Methodology (supporting); Writing – review & editing (supporting). **J.-P. Tetienne:** Data curation (supporting); Funding acquisition (supporting); Investigation (supporting); Methodology (supporting); Resources (supporting); Writing – review & editing (supporting). **E. P. Malkemper:** Conceptualization (supporting); Data curation (supporting); Investigation (supporting); Methodology (supporting); Resources (supporting); Writing – review & editing (supporting). **D. A. Keays:** Conceptualization (supporting); Data curation (supporting); Funding acquisition (supporting); Investigation (supporting); Methodology (supporting); Resources (supporting); Writing – review & editing (supporting). **L. C. L. Hollenberg:** Conceptualization (supporting); Funding acquisition (supporting); Investigation (supporting); Methodology (supporting); Project administration (supporting); Resources (equal); Supervision (supporting); Writing – review & editing (supporting). **D. A. Simpson:** Conceptualization (lead); Data curation (supporting); Formal analysis (supporting); Investigation (equal); Methodology (equal); Project administration (lead); Resources (equal); Supervision (lead); Writing – original draft (equal); Writing – review & editing (equal).

DATA AVAILABILITY

The data that support the findings of this study are available from the corresponding author upon reasonable request.

REFERENCES

[1]P. Jandacka, H. Burda, and J. Pistora, "Magnetically induced behaviour of ferritin corpuscles in avian ears: Can cuticulosomes function as magnetosomes?," J. R. Soc. Interface **12**, 20141087 (2015).

[2]G. C. Papaefthymiou, "The Mössbauer and magnetic properties of ferritin cores," Biochim. Biophys. Acta **1800**, 886–897 (2010).

[3]J. Shaw, A. Boyd, M. House, R. Woodward, F. Mathes, G. Cowin, M. Saunders, and B. Baer, "Magnetic particle-mediated magnetoreception," J. R. Soc. Interface **12**, 20150499 (2015).

[4]J. Clarke, Y.-H. Lee, and J. Schneiderman, "Focus on SQUIDs in biomagnetism," Supercond. Sci. Technol. **31**, 080201 (2018).

[5]D. Passeri, C. Dong, M. Reggente, L. Angeloni, M. Barteri, F. A. Scaramuzzo, F. De Angelis, F. Marinelli, F. Antonelli, F. Rinaldi, C. Marianecci, M. Carafa, A. Sorbo, D. Sordi, I. W. Arends, and M. Rossi, "Magnetic force microscopy: Quantitative issues in biomaterials," Biomatter **4**, e29507 (2014).

[6]B. Chesca, D. John, and R. Cantor, "SQUID-arrays coupled to on-chip integrated thin-film superconducting input coils operating coherently," Appl. Phys. Lett. **118**, 042601 (2021).

[7]M. W. Doherty, N. B. Manson, P. Delaney, F. Jelezko, J. Wrachtrup, and L. C. Hollenberg, "The nitrogen-vacancy colour centre in diamond," Phys. Rep. **528**, 1–45 (2013).

[8]M. H. Alkahtani, F. Alghannam, L. Jiang, A. Almethen, A. A. Rampersaud, R. Brick, C. L. Gomes, M. O. Scully, and P. R. Hemmer, "Fluorescent nanodiamonds: Past, present, and future," Nanophotonics **7**, 1423–1453 (2018).

[9]N. Bondon, L. Raehm, C. Charnay, R. Boukherroub, and J.-O. Durand, "Nanodiamonds for bioapplications, recent developments," J. Mater. Chem. B **8**, 10878–10896 (2020).

[10]S. C. Scholten, A. J. Healey, I. O. Robertson, G. J. Abrahams, D. A. Broadway, and J.-P. Tetienne, "Widefield quantum microscopy with nitrogen-vacancy centers in diamond: Strengths, limitations, and prospects," J. Appl. Phys. **130**, 150902 (2021).

[11]E. Schäfer-Nolte, L. Schlipf, M. Ternes, F. Reinhard, K. Kern, and J. Wrachtrup, "Tracking temperature-dependent relaxation times of ferritin nanomagnets with a wideband quantum spectrometer," Phys. Rev. Lett. **113**, 217204 (2014).

[12]D. L. Sage, K. Arai, D. R. Glenn, S. J. DeVience, L. M. Pham, L. Rahn-Lee, M. D. Lukin, A. Yacoby, A. Komeili, and R. L. Walsworth, "Optical magnetic imaging of living cells," Nature **496**, 486–489 (2013).

[13]D. R. Glenn, R. R. Fu, P. Kehayias, D. L. Sage, E. A. Lima, B. P. Weiss, and R. L. Walsworth, "Micrometer-scale magnetic imaging of geological samples using a quantum diamond microscope," Geochem., Geophys., Geosyst. **18**, 3254–3267, https://doi.org/10.1002/2017GC006946 (2017).

[14]I. Fescenko, A. Laraoui, J. Smits, N. Mosavian, P. Kehayias, J. Seto, L. Bougas, A. Jarmola, and V. M. Acosta, "Diamond magnetic microscopy of malarial hemozoin nanocrystals," Phys. Rev. Appl. **11**, 034029 (2019).

[15]J. M. McCoey, M. Matsuoka, R. W. de Gille, L. T. Hall, J. A. Shaw, J.-P. Tetienne, D. Kisailus, L. C. L. Hollenberg, and D. A. Simpson, "Quantum magnetic imaging of iron biomineralization in teeth of the chiton *Acanthopleura hirtosa*," Small Methods **4**, 1900754 (2020).

[16]R. W. de Gille, J. M. McCoey, L. T. Hall, J.-P. Tetienne, E. P. Malkemper, D. A. Keays, L. C. L. Hollenberg, and D. A. Simpson, "Quantum magnetic imaging of iron organelles within the pigeon cochlea," Proc. Natl. Acad. Sci. **118**, e2112749118 (2021).

[17]M. Capelli, A. Heffernan, T. Ohshima, H. Abe, J. Jeske, A. Hope, A. Greentree, P. Reineck, and B. Gibson, "Increased nitrogen-vacancy centre creation yield in diamond through electron beam irradiation at high temperature," Carbon **143**, 714–719 (2019).

[18]D. J. McCloskey, N. Dontschuk, D. A. Broadway, A. Nadarajah, A. Stacey, J.-P. Tetienne, L. C. L. Hollenberg, S. Prawer, and D. A. Simpson, "Enhanced widefield quantum sensing with nitrogen-vacancy ensembles using diamond nanopillar arrays," ACS Appl. Mater. Interfaces **12**, 13421–13427 (2020).

[19]A. Gruber, A. Dräbenstedt, C. Tietz, L. Fleury, J. Wrachtrup, and C. von Borczyskowski, "Scanning confocal optical microscopy and magnetic resonance on single defect centers," Science **276**, 2012–2014 (1997).

[20]S. Felton, A. M. Edmonds, M. E. Newton, P. M. Martineau, D. Fisher, D. J. Twitchen, and J. M. Baker, "Hyperfine interaction in the ground state of the negatively charged nitrogen vacancy center in diamond," Phys. Rev. B **79**, 075203 (2009).

[21]M. Lauwers, P. Pichler, N. B. Edelman, G. P. Resch, L. Ushakova, M. C. Salzer, D. Heyers, M. Saunders, J. Shaw, and D. A. Keays, "An iron-rich organelle in the cuticular plate of avian hair cells," Curr. Biol. **23**, 924 (2013).

[22]Y. Gossuin, P. Gillis, A. Hocq, Q. L. Vuong, and A. Roch, "Magnetic resonance relaxation properties of superparamagnetic particles," WIREs Nanomed. Nanobiotechnol. **1**, 299–310 (2009).

[23]S. V. Stolyar, O. A. Kolenchukova, A. V. Boldyreva, N. S. Kudryasheva, Y. V. Gerasimova, A. A. Krasikov, R. N. Yaroslavtsev, O. A. Bayukov, V. P. Ladygina, and E. A. Birukova, "Biogenic ferrihydrite nanoparticles: Synthesis, properties in vitro and in vivo testing and the concentration effect," Biomedicines **9**, 323 (2021).

[24]X. Wang, W. Li, R. Harrington, F. Liu, J. B. Parise, X. Feng, and D. L. Sparks, "Effect of ferrihydrite crystallite size on phosphate adsorption reactivity," Environ. Sci. Technol. **47**, 10322–10331 (2013).

[25]P. Jandacka, P. Alexa, J. Pistora, and J. Trojkova, "Hypothetical superparamagnetic magnetometer in a pigeon's upper beak probably does not work," Eur. Phys. J. E **36**, 96 (2013).

[26]S. Nimpf, E. P. Malkemper, M. Lauwers, L. Ushakova, G. Nordmann, A. Wenninger-Weinzierl, T. R. Burkard, S. Jacob, T. Heuser, G. P. Resch, and D. A. Keays, "Subcellular analysis of pigeon hair cells implicates vesicular trafficking in cuticulosome formation and maintenance," eLife **6**, 19 (2017).
[27]S. E. Lillie, D. A. Broadway, N. Dontschuk, S. C. Scholten, B. C. Johnson, S. Wolf, S. Rachel, L. C. L. Hollenberg, and J.-P. Tetienne, "Laser modulation of superconductivity in a cryogenic wide-field nitrogen-vacancy microscope," Nano Lett. **20**, 1855–1861 (2020).
[28]T-h Wu, H. Fu, R. A. Hajjar, T. Suzuki, and M. Mansuripur, "Measurement of magnetic anisotropy constant for magneto-optical recording media: A comparison of several techniques," J. Appl. Phys. **73**, 1368–1376 (1993).
[29]J. Li, W. Wu, Q. Liu, and Y. Pan, "Magnetic anisotropy, magnetostatic interactions and identification of magnetofossils: Toward detection of magnetofossils," Geochem., Geophys., Geosyst. **13**, Q10Z51, https://doi.org/10.1029/2012GC004384 (2012).
[30]T. M. Nocera, J. Chen, C. B. Murray, and G. Agarwal, "Magnetic anisotropy considerations in magnetic force microscopy studies of single superparamagnetic nanoparticles," Nanotechnology **23**, 495704 (2012).